Analytica Chimica Acta 1187 (2021) 339156

Contents lists available at ScienceDirect

Analytica Chimica Acta

journal homepage: www.elsevier.com/locate/aca

Photoelectrochemical monitoring of miRNA based on Au NPs@g-C_3N_4 coupled with exonuclease-involved target cycle amplification

Meng-Jie Li [a, b, *], Si-Yu An [a, b], Ying Wu [a, b]

[a] School of Civil Engineering and Architecture, Chongqing University of Science & Technology, Chongqing, 401331, PR China
[b] Institute for Health and Environment, Chongqing University of Science & Technology, Chongqing, 401331, PR China

HIGHLIGHTS

- Au NPs@g-C_3N_4 with eminent photoelectric property.
- T7 exonuclease-involved target cycle amplification.
- The photoelectrochemical biosensor with sensitive analytical performance for miRNA-141.

GRAPHICAL ABSTRACT

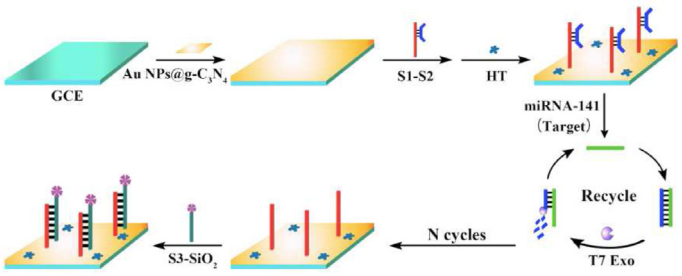

ARTICLE INFO

Article history:
Received 19 August 2021
Received in revised form
4 October 2021
Accepted 5 October 2021
Available online 7 October 2021

Keywords:
Photoelectrochemical biosensor
Au nanoparticles@graphitic-like carbon nitride
SiO_2
microRNA detection
T7 exonuclease
Cycle amplification

ABSTRACT

Herein, a sensitive photoelectrochemical (PEC) biosensing platform was designed for quantitative monitoring of microRNA-141 (miRNA-141) based on Au nanoparticles@graphitic-like carbon nitride (Au NPs@g-C_3N_4) as the signal generator accompanying with T7 exonuclease (T7 Exo)-involved target cycle amplification process. Initially, the prepared Au NPs@g-C_3N_4 as the signal generator was coated on the electrode surface, which could produce a strong PEC signal due to the unique optical and electronic properties of g-C_3N_4 and the surface plasmonic resonance (SPR) enhanced effect of Au NPs. Meanwhile, the modified Au NPs@g-C_3N_4 was also considered as the fixed platform for immobilization of S1−S2 through Au−N bond. Thereafter, the T7 Exo-involved target cycle amplification process would be initiated in existence of miRNA-141 and T7 Exo, leading to abundant single chain S1 exposed on electrode surface. Ultimately, the S3−SiO_2 composite was introduced through DNA hybridization, thereby producing high steric hindrance to block external electrons supply and light harvesting, which would further cause a significantly quenched PEC signal. Experimental results revealed that the PEC signal was gradually inhibited with the raising miRNA-141 concentration in the range from 1 fM to 1 nM with a detection limit of 0.3 fM. The PEC biosensor we proposed here provides a valuable scheme in miRNA assay for early disease diagnosis and biological research.

1. Introduction

As a member of noncoding RNAs, microRNA (miRNA) is single-strand small molecule with a length of 19−23 nucleotides, which is involved in numerous physiological and pathological processes [1,2]. Abundant studies have shown that the abnormal expression

* Corresponding author. School of Civil Engineering and Architecture, Chongqing University of Science & Technology, Chongqing, 401331, PR China.
E-mail address: mengjieli@cqust.edu.cn (M.-J. Li).

https://doi.org/10.1016/j.aca.2021.339156
0003-2670/

of miRNA is closely related to the occurrence and development of human tumor diseases [3–5]. Also, miRNAs have been detected in response to various human diseases, such as infectious disease, kidney disease and heart diseases [6–8]. Therefore, miRNA is recognized as a new and effective diseases diagnostic marker [9]. Concerning the fact that miRNAs possess the inherent characteristics of low content, high similarity among family membership, easy degradation and short size [10,11] it is a real challenge and opportunity to develop a novel method able to quantify easily miRNA with high sensitivity, good stability and strong specificity. Photoelectrochemical (PEC) sensor is a newly emerging and rapidly developed analytical technology that combines the optical signal input with the electrical signal output [12,13]. To date, PEC sensors have been successfully utilized to detect a series of targets due to the merits of high sensitivity, excellent stability and strong specificity [14–16], which might be an excellent candidate for quantification of miRNA.

During the construction of PEC sensor, the choice of photoactive materials is of the essence. Graphitic-like carbon nitride (g-C_3N_4) consisting of green non-toxic and low-cost elements has gained great attention in the fields of biosensing, electrocatalysis and photocatalysis because of its easy processability, chemical stability, excellent electronic conductivity and catalytic activity [17–21]. In particular, the bandgap of g-C_3N_4 (2.7 eV) leads its unique optical and electronic properties [22,23]. Nevertheless, PEC sensor based on the pure g-C_3N_4 has been rarely reported deriving from the fast recombination of its photogenerated electron-hole pairs. Various strategies have been developed to restrain the recombination of electron-hole pairs, which includes constructing heterojunctions, designing sensitized structures, doping with novel elements and combining plasmonic metals [24–27]. Among them, the coupling semiconductor with plasmonic metal has become a common and effective avenue to inhibit recombination and improve photocurrent response. The introduction of plasmonic metals could lead to the occurrence of surface plasmonic resonance (SPR) phenomenon [28]. Concretely, the electromagnetic field of incident light would power the collective oscillation of electrons in metal particles, thereby enhancing the light absorption and the interfacial charge transfer [29]. Accordingly, Au nanoparticles@g-C_3N_4 (Au NPs@g-C_3N_4) with the SPR enhanced effect was synthesized and adopted in this work, which presented eminent photoelectric property and could be utilized as the excellent PEC signal generator.

Herein, a sensitive PEC biosensing platform based on Au NPs@g-C_3N_4 as the signal generator coupling with T7 exonuclease (T7 Exo)-involved target cycle amplification process was proposed for quantitative monitoring of microRNA-141 (miRNA-141), which was designed as Scheme 1. Initially, the prepared Au NPs@g-C_3N_4 with excellent PEC property was coated on electrode surface, generating a strong photocurrent response. After immobilization of S1–S2 *via* Au–N bond, the blocking agent (hexanethiol, HT) was incubated. Afterwards, miRNA-141 and T7 Exo were added, in which miRNA-141 could hybridize with S2 to trigger the subsequent digestion by T7 Exo. S2 was digested to abundant mononucleotides and miRNA-141 was released to hybridize with the next S2. With the aid of T7 Exo-involved target cycle amplification, small amounts of miRNA-141 were converted into abundant single chain S1. Ultimately, the S3–SiO_2 composite was introduced through the hybridization between S1 and S3, leading to the high steric hindrance, thereby directly blocking external electrons supply and light harvesting. In consequence, the photocurrent response of Au NPs@g-C_3N_4 was gradually inhibited with the raising miRNA-141 concentration, which would be recorded to quantitatively determine the concentration of miRNA-141. The PEC biosensing platform we designed here not only expanded the application of Au NPs@g-C_3N_4 in bioanalysis but also devoted a new routine for sensitive monitoring of miRNA.

2. Experimental section

2.1. Synthesis of Au NPs@g-C_3N_4

g-C_3N_4 was synthesized as previously reported [30]. Firstly, 5 g melamine was added in a crucible and dried at 80 °C for 24 h in atmospheric air. Next, the intermediate product was transferred into a muffle furnace, followed by calcinating at 550 °C for 3 h with a ramp of 5 °C/min. Finally, residual alkaline impurities were removed by centrifugation with nitric acid and ultrapure water. The light yellow product (g-C_3N_4) was obtained and stored in refrigerator for subsequent use.

For preparation of Au NPs@g-C_3N_4 [31], 20 μL $HAuCl_4$ aqueous solution (10 mM) and 5 mL g-C_3N_4 aqueous solution (2 mg/mL) were mixed, followed by stirring for 2 h in the dark. Afterwards, 30 μL the freshly prepared $NaBH_4$ solution (0.01 M) was added dropwise to the above solution with continuously stirring. The reaction was complete until the gas evolution stopped. Finally, the obtained Au NPs@g-C_3N_4 was washed by centrifugation, and redispersed in 5 mL ultrapure water for subsequent use.

2.2. Synthesis of SiO_2 and S3–SiO_2 composites

SiO_2 particles were obtained as previously reported [32]. Briefly, 6 mL ultrapure water, 16.5 mL ethanol and 2 mL $NH_3 \cdot H_2O$ were mixed and stirred continuously to get homogeneous solution. After 20 min, 18.5 mL ethanol solution dispersed with 2 mL tetraethoxysilane (TEOS) was added, and the mixture was stirred for 15 h at 30 °C. SiO_2 particles were centrifugally washed with ethanol for

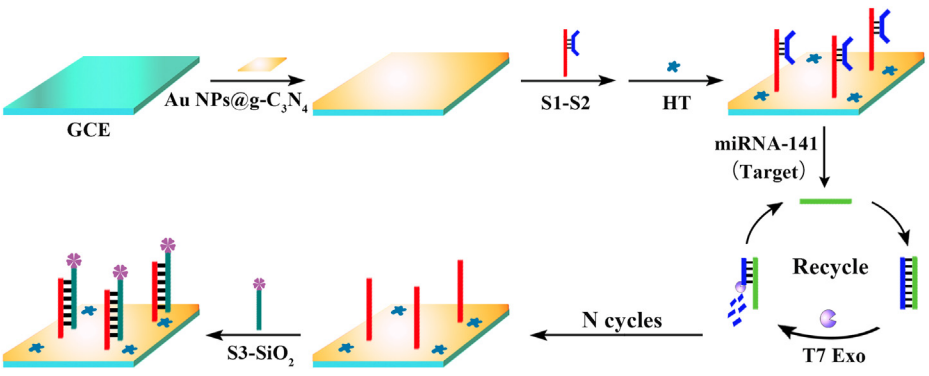

Scheme 1. Schematic illustration of the PEC biosensing platform for miRNA assay.

three times and then dispersed in ethanol.

Amino-modified SiO_2 particles (SiO_2—NH_2) were prepared according to the literature [32]. 0.5 mL 3-aminopropyl triethoxysilane (APTES) and 30 mL the prepared SiO_2 particles were mixed and vigorously stirred. Subsequently, the mixture was heated to 76 °C under refluxing for over 24 h. The product (SiO_2—NH_2) was centrifugally cleaned with ethanol for several times. Finally, SiO_2—NH_2 were dispersed in ultrapure water and stored at 4 °C.

For preparation of S3—SiO_2 composite, 30 μL SiO_2—NH_2, 10 μL 0.05% glutaraldehyde and 1 mL 2 μM amino-terminated S3 were mixed and stirred continuously for 2 h at room temperature to complete the crosslinking reaction [33]. The obtained S3—SiO_2 composite was purified by centrifugation, and then redispersed in 1 mL PBS for subsequent use.

2.3. Construction of PEC biosensing platform

First of all, 15 μL Au NPs@g-C_3N_4 (2 mg/mL) was coated on glassy carbon electrode (GCE) surface and dried at 37 °C to obtain Au NPs@g-C_3N_4/GCE. Next, 20 μL the prepared S1—S2 (2 μM) was dropped on the surface of Au NPs@g-C_3N_4/GCE and kept for 12 h, which could be steadily immobilized *via* Au—N bond. Subsequently, 10 μL hexanethiol (HT, 0.1 mM) was incubated for 30 min to block nonspecific sites. Afterwards, the electrode was incubated with 20 μL of various concentrations target (miRNA-141) and 100 U/mL T7 Exo for 90 min at 25 °C. As shown in Scheme 1, T7 Exo-involved miRNA-141 cycle amplification process would be triggered. Concretely, miRNA-141 would displace S1 to form the duplex of miRNA-141/S2, which could be cleaved by T7 Exo from 5′ to 3′ direction. As a result, S2 was digested to mononucleotides, and miRNA-141 was released to displace the next S1. After N cycles, abundant single chain S1 were exposed on electrode surface. Finally, 20 μL the prepared S3—SiO_2 composite was coated on the obtained GCE surface for 2 h at 37 °C. Scheme 1 illustrated the construction procedure of this PEC biosensing platform.

3. Results and discussions

3.1. Characterization of the different nanomaterials

The morphologies of g-C_3N_4, Au NPs@g-C_3N_4 and SiO_2 particles were detected by scanning electron microscopy (SEM), and the elements of Au NPs@g-C_3N_4 were characterized by energy dispersive X-ray (EDX) spectrum. As revealed in Fig. 1A, the morphology of the synthesized g-C_3N_4 was two dimensional haze structure. After modification with Au NPs, it could be clearly found that many nanoparticles were evenly embellished on the g-C_3N_4 surface (Fig. 1B). To further confirm the successful synthesis of Au NPs@g-C_3N_4, the concrete elements were recorded by the EDX spectrum. As shown in Fig. 2, the elements of Au, C, N and Si could be distinctly observed, in which Au, C and N were supplied by Au NPs@g-C_3N_4 and the element of Si originated from the immobilized substrate (silicon slice). Besides, the SEM image of SiO_2 particles was recorded in Fig. 1C. The SiO_2 particles possessed the uniform spherical structure about 350 nm in size, indicating that the SiO_2 particles were successfully formed.

3.2. PEC mechanism of the biosensor

Fig. 3A presented the photocurrent generating mechanism with the Au NPs@g-C_3N_4 modified on the GCE surface. Initially, the electrons migrated from the valence band (VB) of g-C_3N_4 to its conduction band (CB) under the visible-light irradiation. Part of electrons located in CB rapidly transported to electrode, and the other part of electrons could immediately move to Au NPs owing to the interface built between Au NPs and g-C_3N_4. Meanwhile, the electromagnetic field of incident light would power the collective oscillation of electrons in Au NPs because of the existence of SPR enhanced effect, and then these oscillated electrons would rapidly transfer to electrode. Electron donor (H_2O_2) in electrolyte solution would continuously supply electrons to the VB of g-C_3N_4. All of these processes would promote the separation of electrons and holes, leading to a strong photocurrent response. Fig. 3B presented the photocurrent quenching mechanism after modification with the S3—SiO_2 composite. Concretely, the introduced SiO_2 particles through DNA hybridization could produce the high steric hindrance on the surface of electrode. The SiO_2 particles not only hindered the light harvesting but also directly blocked the external electrons supply [34]. As a consequence, the photocurrent response of Au NPs@g-C_3N_4 would be substantially quenched.

3.3. PEC characterization of the biosensor

To assess the availability of the fabricated PEC sensor, the photocurrents at different preparation stages were recorded in Fig. 4. Clearly, a background photocurrent close to zero for bare GCE was observed (curve a). The photocurrent increased sharply to the maximum when Au NPs@g-C_3N_4 was coated on GCE surface (curve b) because of its excellent photoelectric properties. With S1—S2 (curve c) and HT (curve d) continuously assembled on the above GCE surface, the photocurrent responses decreased successively since their charge transfer ability were poor. Ultimately, a significantly reduced photocurrent response was obtained (curve e) after incubating with S3—SiO_2, T7 Exo and miRNA-141, which contributed to the fact that the SiO_2 introduced by DNA hybridization could block electron transfer and effectively quench the photocurrent of Au NPs@g-C_3N_4. These results suggested that the stepwise construction process of this biosensor was successful.

3.4. Electrochemical characterization of the PEC biosensor

To characterize the PEC biosensor preparation procedure step by step, cyclic voltammetry (CV) measurement was conducted in 2 mL PBS (pH 7, 0.1 M) containing 5.0 mM $[Fe(CN)_6]^{3-/4-}$ and 0.1 M KCl between −0.2 and 0.6 V at a scan rate of 50 mV/s. As displayed in Fig. 5A, the bare GCE (curve a) exhibited a pair of reversible redox peaks. After the immobilization of Au NPs@g-C_3N_4 on GCE, the peak current decreased (curve b) caused by the semiconductor properties of Au NPs@g-C_3N_4. The introduction of S1—S2 induced the further decrease of peak current (curve c), owing to the electronic repulsion between $[Fe(CN)_6]^{3-/4-}$ and the negatively charged S1—S2. Next, HT was modified on the resultant GCE to block the nonspecific binding sites, resulting in a continued decrease of the peak current (curve d). Finally, when S3—SiO_2, T7 Exo and miRNA-141 were incubated on the surface of the electrode, the peak current was further weakened (curve e), which contributed to the fact that the increased steric hindrance effect and the hybridization between S3—SiO_2 and S1 blocked the electron transfer.

Meanwhile, as shown in Fig. 5B, electrochemical impedance spectroscopy (EIS) measurement was employed to characterize the fabrication of PEC biosensor. EIS measurement was recorded in 2 mL PBS (pH 7.0, 0.1 M) containing 5.0 mM $[Fe(CN)_6]^{3-/4-}$ and 0.1 M KCl over a frequency range of 10 kHz to 0.1 Hz using an alternating current potential with an amplitude of 5 mV at a direct current potential of 0.22 V. The charge-transfer resistance (R_{et}) for bare GCE was the curve a. The R_{et} of the GCE modified with Au NPs@g-C_3N_4 increased obviously (curve b), which may be due to the fact that the modified Au NPs@g-C_3N_4 hindered the electron transfer. When the S1—S2 was fixed on the Au NPs@g-C_3N_4/GCE, the R_{et} continued to increase (curve c) due to the poor electrical

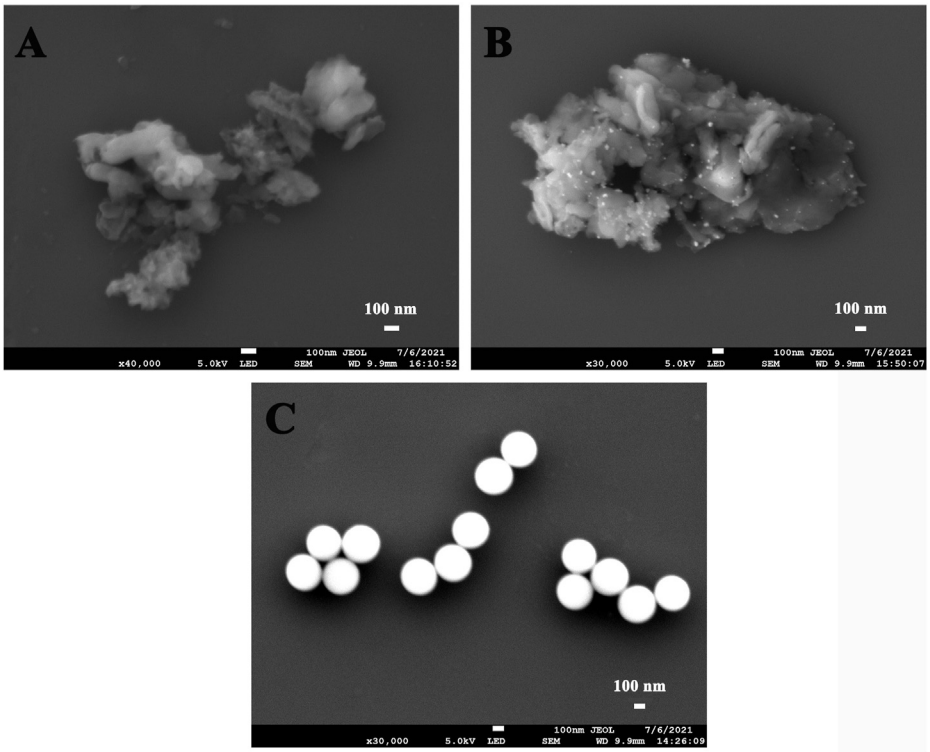

Fig. 1. SEM images of g-C_3N_4 (A), Au NPs@g-C_3N_4 (B) and SiO_2 particles (C).

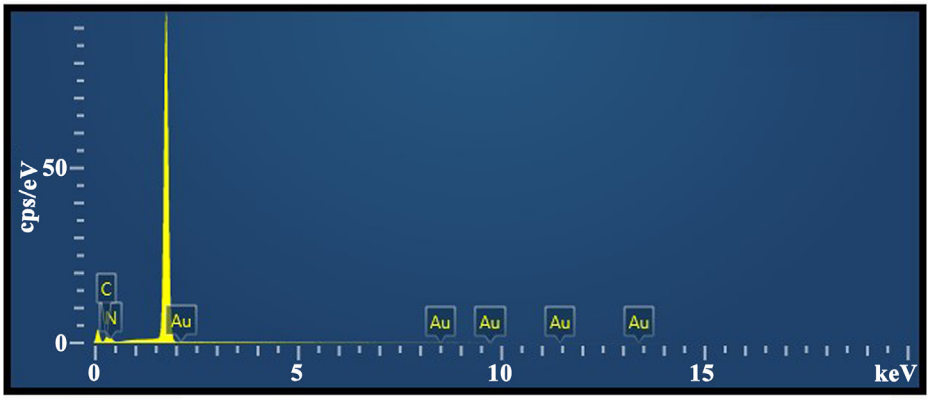

Fig. 2. EDX spectrum of Au NPs@g-C_3N_4.

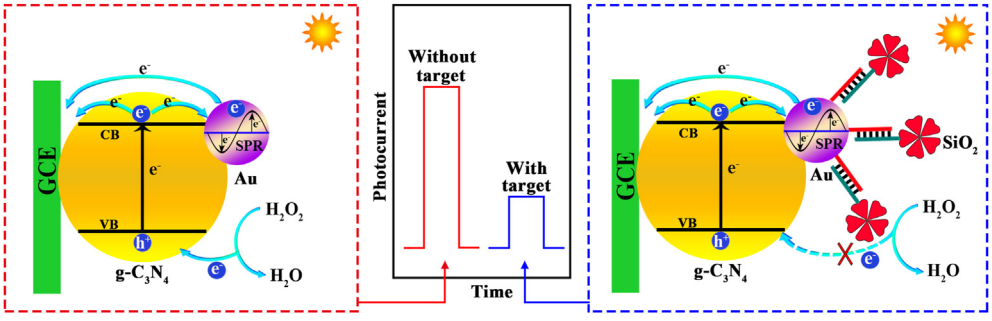

Fig. 3. Schematic illustration of the photocurrent generating (A) and quenching (B) mechanisms.

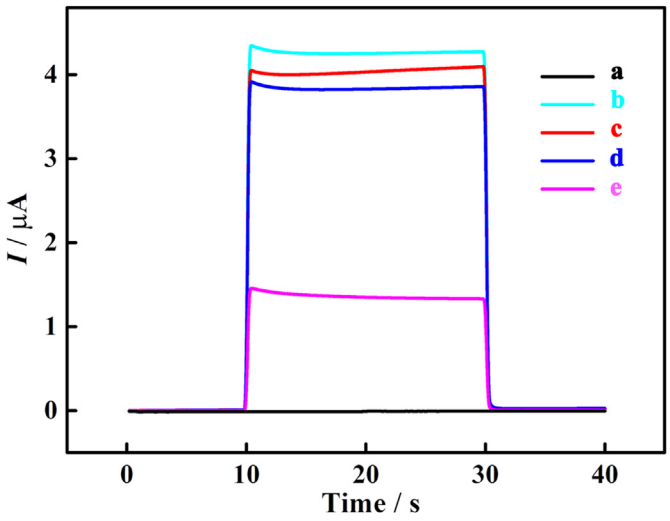

Fig. 4. Photocurrent signal of (a) bare GCE, (b) Au NPs@g-C_3N_4/GCE, (c) S1−S2/Au NPs@g-C_3N_4/GCE, (d) HT/S1−S2/Au NPs@g-C_3N_4/GCE and (e) S3−SiO_2/T7 Exo/miRNA-141/HT/S1−S2/Au NPs@g-C_3N_4/GCE.

conductivity of the DNA sequence. After incubation of non-conductive HT, the R_{et} increased obviously (curve d). A further increase of the R_{et} was found after incubating with S3−SiO_2, T7 Exo and miRNA-141 (curve e) because of the increased steric hindrance effect. These results manifested the successful preparation of the PEC biosensor.

3.5. Detection of miRNA-141

To evaluate the analytical performance of the presented PEC sensing platform, the photocurrent signals were measured toward a series of miRNA-141 concentrations under the optimal conditions, which was shown in Fig. 6A. It was found that the photocurrent signal decreased dramatically along with the increase of miRNA-141 concentration from 1 fM to 1 nM. Fig. 6B showed the linear response curve between the photocurrent signal (I) and the logarithm of miRNA-141 concentration (lg$c$) with a linear regression equation of $I = -0.3633 \lg c + 1.481$ and a correlation coefficient of 0.9925. Besides, the calculated detection limit was 0.3 fM and the calculation method was derived from reference. [35] Meanwhile, the analytical performances of the proposed PEC biosensor were compared to some previously reported methods. In order to ensure the rationality of comparison, these methods selected for comparison used only one amplification technique because only one amplification strategy was adopted in the proposed PEC biosensor. As seen in Table 1, an improved sensitivity and a much wider linear range were observed in our work, which indicated that this work performed a prominent analytical performance for miRNA-141 detection. Besides, some works for miRNA detection possessed the detection limit as low as aM level, which was attribute to the application of double or even triple signal amplification strategies. The related contents were presented in Table S1 (Electronic Supplementary Material).

3.6. Stability and selectivity of the PEC biosensor

In order to explore the stability, PEC biosensor incubated with 0.1 nM miRNA-141 was monitored for 10 cycles under continuous "off-on-off" light. Fairly stable PEC signals could be caught from

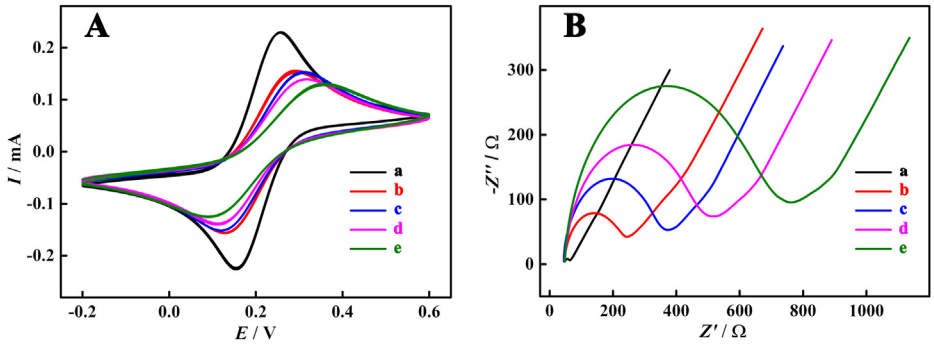

Fig. 5. CV (A) and EIS (B) responses of (a) bare GCE, (b) Au NPs@g-C_3N_4/GCE, (c) S1−S2/Au NPs@g-C_3N_4/GCE, (d) HT/S1−S2/Au NPs@g-C_3N_4/GCE and (e) S3−SiO_2/T7 Exo/miRNA-141/HT/S1−S2/Au NPs@g-C_3N_4/GCE.

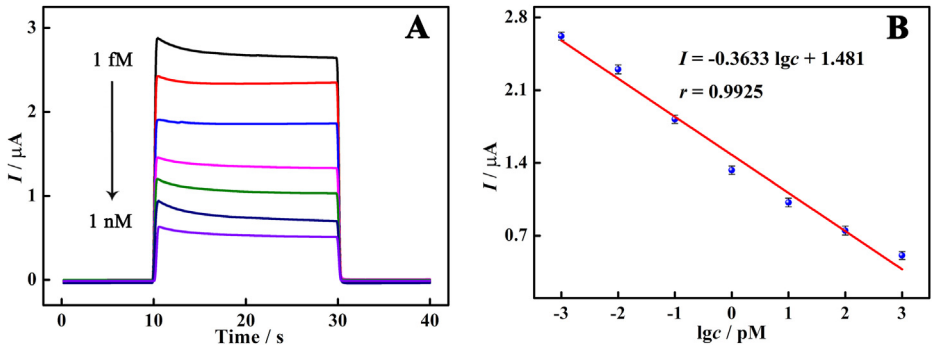

Fig. 6. (A) Photocurrent signals with various miRNA-141 concentrations. (B) Linear relationship between the photocurrent signals and the logarithm of miRNA-141 concentration.

Table 1
Comparison of different methods for miRNA detection.

Method	Technique	LOD	Linear range	Ref.
fluorescence	DSN assisted target recycling	33.4 fM	100 fM-1 nM	[36]
ECL	hybridization chain reaction	2 fM	5 fM-5 pM	[37]
colorimetry	DSN assisted target recycling	44.76 fM	50 fM-3000 fM	[38]
electrochemistry	DNAzyme-cleavage cycling	1.8 fM	10 fM-0.1 nM	[39]
CL	cross-catalyst SDA	0.68 fM	1 fM-10 fM	[40]
PEC	toehold-mediated SDA	0.5 fM	1 fM-10 pM	[13]
PEC	T7 Exo-involved target cycle	0.3 fM	1 fM-1 nM	Our work

Abbreviations: duplex-specific nuclease (DSN); strand displacement amplification (SDA); electrochemiluminescence (ECL); chemiluminescence (CL).

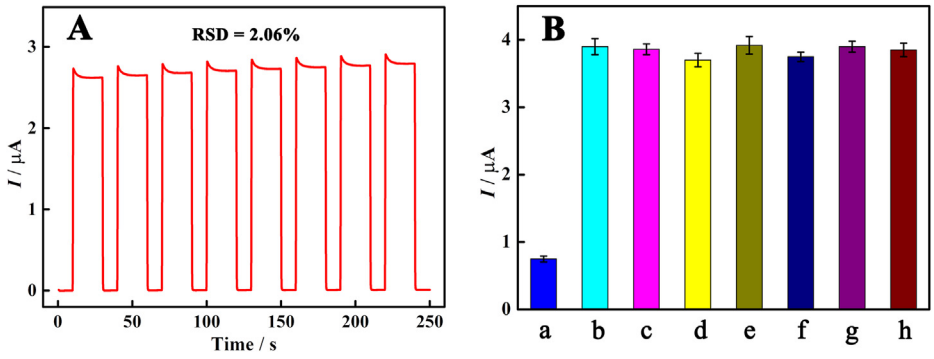

Fig. 7. (A) Stability test of the biosensor at 0.1 nM miRNA-141. (B) Selectivity of the biosensor to miRNA-141 (column a) with 0.1 nM by comparison to the interferences at the 10 nM level: b (blank), c (thrombin), d (miRNA-21), e (miRNA-155), f (single-base mismatched sequence), g (double-base mismatched sequence) and h (triple-base mismatched sequence).

Fig. 7A and the relative standard deviation (RSD) of 2.06% could be calculated, meaning that the proposed PEC biosensor possessed a good stability for the detection of miRNA-141. Furthermore, the selectivity of the designed strategy toward miRNA-141 was also studied through utilizing thrombin, miRNA-21, miRNA-155, single, double, triple-base mismatched sequences as interferences. From Fig. 7B, strong PEC signals were found in existence of 10 nM interferences, which was the same as the blank detection. However, when 0.1 nM miRNA-141 was used as the detection sample, the PEC signal reduced significantly. The result revealed a satisfied selectivity toward miRNA-141 detection of the designed strategy.

3.7. Detection of miRNA-141 in human serum samples

To evaluate the preliminary application ability of the proposed PEC biosensor, the human serum samples were used as the sample matrixes to detect miRNA-141 through the standard addition method. The human serum samples were isolated from the whole blood by the centrifugation at 3000 rpm for 20 min and then stored at −80 °C for further use. MiRNA-141 with different concentrations were added into 50-fold-diluted human serum samples and then detected by this PEC biosensor. The experimental results were expected in Table 2. The recoveries varied from 95.00 to 106.00% with relative standard deviation (RSD, n = 8) between 3.50% and 6.20%, indicating that the proposed PEC biosensor possessed excellent application ability for miRNA-141 detection in human serum samples.

Table 2
Detection of miRNA-141 in human serum samples.

Sample number	Added (pM)	Found (pM)	Recovery (%)	RSD (%)
1	5.00×10^{-2}	4.80×10^{-2}	96.00	5.20
2	5.00×10^{-1}	5.30×10^{-1}	106.00	6.20
3	5.00	5.10	102.00	3.50
4	50.00	47.50	95.00	4.20
5	500.00	490.00	98.00	3.90

4. Conclusion

In summary, a PEC biosensor for sensitive assay of miRNA-141 was proposed on the basis of Au NPs@g-C_3N_4 as the PEC signal generator coupling with T7 Exo-involved target cycle amplification process. The synthesized Au NPs@g-C_3N_4 could produce a strong PEC signal owing to the unique optical and electronic properties of g-C_3N_4 and the surface plasmonic resonance (SPR) enhanced effect of Au NPs. Besides, the introduction of T7 Exo-involved target cycle amplification could convert a handful of miRNA-141 into abundant single chain S1 for further hybridize with S3—SiO_2, which could significantly quench PEC signal and tremendously improve analytical sensitivity during the detection of miRNA-141. The designed PEC biosensing platform offers a new opportunity for application of Au NPs@g-C_3N_4 in bioanalysis and provides a novel method for sensitive monitoring of miRNA.

CRediT authorship contribution statement

Meng-Jie Li: Experimental testing, Data curation, Writing – original draft, Conceptualization, Methodology. **Si-Yu An:** Software, Investigation. **Ying Wu:** Writing – review & editing.

Declaration of competing interest

The authors declare that they have no known competing financial interests or personal relationships that could have appeared to influence the work reported in this paper.

Acknowledgement

This work was financially supported by Science and technology

research project of Chongqing education commission (KJQN202101522) and Research start-up fund for new faculty of Chongqing university of Science and Technology (ckrc2020024).

Appendix A. Supplementary data

Supplementary data to this article can be found online at https://doi.org/10.1016/j.aca.2021.339156.

References

[1] Z.Q. Ning, E.L. Yang, Y.J. Zheng, M.Y. Chen, G.Q. Wu, Y.J. Zhang, Y.F. Shen, A dual functional self-enhanced electrochemiluminescent nanohybrid for label-free microRNA detection, Anal. Chem. 93 (2021) 8971–8977.

[2] B.M. Ryan, A.I. Robles, C.C. Harris, Genetic variation in microRNA networks: the implications for cancer research, Nat. Rev. Cancer 10 (2010) 389–402.

[3] H.F. Dong, J.P. Lei, L. Ding, Y.Q. Wen, H.X. Ju, X.J. Zhang, MicroRNA: function, detection, and bioanalysis, Chem. Rev. 113 (2013) 6207–6233.

[4] D.P. Bartel, MicroRNAs: genomics, biogenesis, mechanism, and function, Cell 116 (2004) 281–297.

[5] R.Y. Yang, G.H. Jiang, H.M. Liu, L.L. He, F. Yu, L.E. Liu, L.B. Qu, Y.J. Wu, A dual-model "on-super off" photoelectrochemical/ratiometric electrochemical biosensor for ultrasensitive and accurate detection of microRNA-224, Biosens. Bioelectron. 188 (2021) 113337.

[6] H.V. Tran, B. Piro, S. Reisberg, H.T. Duc, M.C. Pham, Antibodies directed to RNA/DNA hybrids: an electrochemical immunosensor for microRNAs detection using graphene-composite electrodes, Anal. Chem. 85 (2013) 8469–8474.

[7] L. Tribolet, E. Kerr, C. Cowled, A.G.D. Bean, C.R. Stewart, M. Dearnley, R.J. Farr, MicroRNA biomarkers for infectious diseases: from basic research to biosensing, Front. Microbiol. 11 (2020) 1197.

[8] T. Papadopoulos, J. Belliere, J.L. Bascands, E. Neau, J. Klein, J.P. Schanstra, miRNAs in urine: a mirror image of kidney disease? Expert Rev. Mol. Diagn. 15 (2015) 361–374.

[9] L. Li, Y. Zhang, Z. Yan, M.Q. Chen, L.N. Zhang, P.N. Zhao, J.H. Yu, Ultrasensitive photoelectrochemical detection of microRNA on paper by combining a cascade nanozyme-engineered biocatalytic precipitation reaction and target-triggerable DNA motor, ACS Sens. 5 (2020) 1482–1490.

[10] M. Labib, S.M. Ghobadloo, N. Khan, D.M. Kolpashchikov, M.V. Berezovski, Four-qay junction formation promoting ultrasensitive electrochemical detection of microRNA, Anal. Chem. 85 (2013) 9422–9427.

[11] A.Y. Chen, G.F. Gui, Y. Zhuo, Y.Q. Chai, Y. Xiang, R. Yuan, Signal-off electrochemiluminescence biosensor based on phi29 DNA polymerase mediated strand displacement amplification for microRNA detection, Anal. Chem. 87 (2015) 6328–6334.

[12] H.B. Li, M. Han, X. Weng, Y.Y. Zhang, J. Li, DNA-tetrahedral-nanostructure-based entropy-driven amplifier for high-performance photoelectrochemical biosensing, ACS Nano 15 (2021) 1710–1717.

[13] N. Zhang, X.M. Shi, H.Q. Guo, X.Z. Zhao, W.W. Zhao, J.J. Xu, H.Y. Chen, Gold nanoparticle couples with entropy-driven toehold-mediated DNA strand displacement reaction on magnetic beads: toward ultrasensitive energy-transfer-based photoelectrochemical detection of miRNA-141 in real blood sample, Anal. Chem. 90 (2018) 11892–11898.

[14] A. Blidar, S. Trashin, E.N. Carrión, S.M. Gorun, C. Cristea, K.D. Wael, Enhanced photoelectrochemical detection of an analyte triggered by its concentration by a singlet oxygen-generating fluoro photosensitizer, ACS Sens. 5 (2020) 3501–3509.

[15] X.Y. Yang, M.J. Zhang, Z.X. Chen, Y.W. Bu, X. Gao, Y.K. Sui, Y.Q. Yu, Sodium alginate micelle-encapsulating zinc phthalocyanine dye-sensitized photoelectrochemical biosensor with CdS as the photoelectric material for Hg^{2+} detection, ACS Appl. Mater. Interfaces 13 (2021) 16828–16836.

[16] Q. Cheng, J.H. Feng, T.T. Wu, Y.J. Guo, X. Sun, X. Ren, Y.J. Lee, L. Liu, Q. Wei, Hollow performances quenching label of Au NPs@$CoSnO_3$ nanoboxes-based sandwich photoelectrochemical immunosensor for sensitive CYFRA 21-1 detection, Talanta 233 (2021) 122552.

[17] Y. Zheng, Y. Jiao, Y.H. Zhu, Q.R. Cai, A. Vasileff, L.H. Li, Y. Han, Y. Chen, S.Z. Qiao, Molecule-level g-C_3N_4 coordinated transition metals as a new class of electrocatalysts for oxygen electrode reactions, J. Am. Chem. Soc. 139 (2017) 3336–3339.

[18] R.Y. Li, Y. Zhang, W.W. Tu, Z.H. Dai, Photoelectrochemical bioanalysis platform for cells monitoring based on dual signal amplification using in situ generation of electron acceptor coupled with heterojunction, ACS Appl. Mater. Interfaces 9 (2017) 22289–22297.

[19] E. Lee, Y. Jun, W. Hong, A. Thomas, M. Jin, Cubic mesoporous graphitic carbon (IV) nitride: an all-in-one chemo-sensor for selective optical sensing of metal ions, Angew. Chem. Int. Ed. 49 (2010) 9706–9710.

[20] M. Ghalkhani, H. Charkhan, M. Sabbaghan, Synthesis and application of a powerful heterogeneous photo-Fenton catalyst based on rGO/g-C3N4/Fe3O4/TiO2 nano-composite for the removal of sewage contaminants, J. Electrochem. Soc. 167 (2020), 067515.

[21] M. Ghalkhani, M.H. Khaneghah, E. Sohouli, Chapter 13: graphitic carbon nitride: synthesis and characterization, Handbook of Carbon-Based Nanomaterials (2021) 573–590.

[22] Z.W. Tong, D. Yang, Z. Li, Y.H. Nan, F. Ding, Y.C. Shen, Z.Y. Jiang, Thylakoid-inspired multishell g-C_3N_4 nanocapsules with enhanced visible-light harvesting and electron transfer properties for high-efficiency photocatalysis, ACS Nano 11 (2017) 1103–1112.

[23] Z.X. Cai, M.C. Rong, T.T. Zhao, L. Zhao, Y.R. Wang, X. Chen, Solar-induced photoelectrochemical sensing for dopamine based on TiO_2 nanoparticles on g-C_3N_4 decorated graphene nanosheets, J. Electroanal. Chem. 759 (2015) 32–37.

[24] J.X. Low, J.G. Yu, M. Jaroniec, S. Wageh, A.A. Al-Ghamdi, Heterojunction photocatalysts, Adv. Mater. 29 (2017) 1601694.

[25] Y.C. Park, E.H. Kong, Y.J. Chang, B.G. Kum, H.M. Jang, Tertiary hierarchically structured TiO_2 for CdS quantum-dot-sensitized solar cells, Electrochim. Acta 56 (2011) 7371–7376.

[26] N. Hao, X. Zhang, Z. Zhou, J. Qian, Q. Liu, S.B. Chen, Y. Zhang, K. Wang, Three-dimensional nitrogen-doped graphene porous hydrogelfabricated biosensing platform with enhanced photoelectrochemical performance, Sensor. Actuator. B Chem. 250 (2017) 476–483.

[27] C.C. Peng, W.Z. Wang, W.W. Zhang, Y.J. Liang, L. Zhuo, Surface plasmon-driven photoelectrochemical water splitting of TiO_2 nanowires decorated with Ag nanoparticles under visible light illumination, Appl. Surf. Sci. 420 (2017) 286–295.

[28] Y.Y. Shi, G.Q. Zhang, J.J. Li, Y. Zhang, Y.B. Yu, Q. Wei, Photoelectrochemical determination of Hg(II) via dual signal amplification involving SPR enhancement and a folding-based DNA probe, Microchim Acta 184 (2017) 1379–1387.

[29] K.Y. Guo, Z.F. Liu, J.H. Han, X.Q. Zhang, Y.J. Li, T.T. Hong, C.L. Zhou, Higher-efficiency photoelectrochemical electrodes of titanium dioxide-based nanoarrays sensitized simultaneously with plasmonic silver nanoparticles and multiple metal sulfides photosensitizers, J. Power Sources 285 (2015) 185–194.

[30] H.M. Da, H.Y. Liu, Y.N. Zheng, R. Yuan, Y.Q. Chai, A highly sensitive $VEGF_{165}$ photoelectrochemical biosensor fabricated by assembly of aptamer bridged DNA networks, Biosens. Bioelectron. 101 (2018) 213–218.

[31] J.Y. Zhuang, W.Q. Lai, M.D. Xu, Q. Zhou, D.P. Tang, Plasmonic AuNP/g-C_3N_4 nanohybrid-based photoelectrochemical sensing platform for ultrasensitive monitoring of polynucleotide kinase activity accompanying DNAzyme-catalyzed precipitation amplification, ACS Appl. Mater. Interfaces 7 (2015) 8330–8338.

[32] Z.Z. Yang, X. Peng, P. Yang, Y. Zhuo, Y.Q. Chai, W.B. Liang, R. Yuan, A Janus 3D DNA nanomachine for simultaneous and sensitive fluorescence detection and imaging of dual microRNAs in cancer cells, Chem. Sci. 11 (2020) 8482–8488.

[33] Y.N. Zheng, W.B. Liang, C.Y. Xiong, Y.L. Yuan, Y.Q. Chai, R. Yuan, Self-enhanced ultrasensitive photoelectrochemical biosensor based on nanocapsule packaging both donor-acceptor-type photoactive material and its sensitizer, Anal. Chem. 88 (2016) 8698–8705.

[34] H. Zare, M. Ghalkhani, O. Akhavan, N. Taghaviniad, M. Marandi, Highly sensitive selective sensing of nickel ions using repeatable fluorescence quenching-emerging of the CdTe quantum dots, Mater. Res. Bull. 95 (2017) 532–538.

[35] A.E. Radi, J.L.A. Sánchez, E. Baldrich, C.K. O'Sullivan, Reagentless, reusable, ultrasensitive electrochemical molecular beacon aptasensor, J. Am. Chem. Soc. 128 (2006) 117–124.

[36] X.M. Miao, Z.Y. Cheng, H.Y. Ma, Z.B. Li, N. Xue, P. Wang, Label-free platform for microRNA detection based on the fluorescence quenching of positively charged gold nanoparticles to silver nanoclusters, Anal. Chem. 90 (2018) 1098–1103.

[37] Y.J. Zheng, Y.C. Xu, L. Chen, X.Y. Yin, F. Lin, S.H. Weng, X.H. Lin, Dual-modal biosensor for the determination of femtomolar miRNA-126 based on electrochemical impedance spectroscopy and electrochemiluminescence with hybridization chain reaction amplification, J. Electrochem. Soc. 167 (2020) 167502.

[38] Y.K. Xia, T.T. Chen, L. Zhang, X.L. Zhang, W.H. Shi, G.Y. Chen, W.Q. Chen, J.M. Lan, C.Y. Li, W.M. Sun, J.H. Chen, Colorimetric detection of exosomal microRNA through switching the visible-light-induced oxidase mimic activity of acridone derivate, Biosens. Bioelectron. 173 (2021) 112834.

[39] X.Y. Lin, J.J. Jiang, J. Wang, J.L. Xia, R.N. Wang, G.W. Diao, Competitive host-guest recognition initiated by DNAzyme-cleavage cycling for novel ratiometric electrochemical assay of miRNA-21, Sensor. Actuator. B Chem. 333 (2021) 129556.

[40] S. Bi, J. Zhang, S. Hao, C. Ding, S.S. Zhang, Exponential amplification for chemiluminescence resonance energy transfer detection of microRNA in real samples based on a cross-catalyst strand-displacement network, Anal. Chem. 83 (2011) 3696–3702.